0267-7261(95)00001-1

# Azimuth dependent wave amplification in alluvial valleys

## H. A. Pedersen,[a] M. Campillo[a,b] & F. J. Sánchez-Sesma[c]

[a]*Laboratoire de Géophysique Interne et Tectonophysique, Université Joseph Fourier, BP 53x, F-38041 Grenoble Cedex, France*
[b]*Institut Universitaire de France,* [c]*Instituto de Ingeniería, UNAM, Cd Universitaria, Apdo 70-472, Coyoacán 04510, México D.F., México and Centro de Investigación Sísmica, Carr al Ajusco 203, Col H de Padierna, Tlalpan 14200, México D.F., México*

An extension of the indirect boundary element method (IBEM) to three-dimensional scattering by two-dimensional alluvial valleys is presented. While the valley is two-dimensional, the incident plane waves can arrive outside the 2D plane so the scattering is three-dimensional with coupling of P–SV–SH waves. Such a method makes it possible to take earthquake location into account in the estimation of site effects in alluvial valleys. The method is validated by transparency tests, by comparison with 2D simulations, and by comparison with results of other authors. The advantage of the method is that it combines high accuracy with cost-efficiency in terms of computer-time. It is applied to theoretically estimate site effects across a simplified model of an alluvial valley in the French Alps where azimuth dependence of local amplification has been observed. A parametric study with simulations for a range of azimuths and incidence angles shows that (1) the local amplification depends strongly on both azimuth and incidence of the incoming waves, (2) the global pattern of amplification across the valley is very complex for all azimuths, and (3) it is not possible to predict the 3D response of the valley from 2D modeling. Theoretical spectral ratios are in approximate agreement with observed ones for a station in the center of the valley where the local structure justifies use of a simplified model for the comparison.

*Key words:* site effects, azimuth dependence, boundary methods, 2·5D diffraction.

## INTRODUCTION

Over the last decade, the importance of local amplification in sedimentary basins has been well established by a large number of observations (e.g. Rogers *et al.*,[1] Tucker and King,[2] Singh *et al.*,[3] Jongmans and Campillo,[4] Borcherdt and Glassmoyer,[5] Gutierrez and Singh.[6] Some wave propagation phenomena relevant to the local amplification have been identified in observations and numerical simulations (e.g. Bard and Bouchon,[7,8] Kawase and Aki,[9] Phillips *et al.*,[10] Sánchez-Sesma *et al.*[11]).

Two-dimensional (2D) numerical simulations show that the amplification pattern is very complex even in simple valleys. Therefore, in order to improve quantitative interpretations of observations of local amplification, it is in most cases necessary to consider more complete models. Considerable effort has been made to extend the modeling to three-dimensional (3D) basins (e.g. Lee and Langston,[12] Sánchez-Sesma,[13] Sánchez-Sesma *et al.*,[14] Frankel and Vidale,[15] Rial,[16] Sánchez-Sesma and

Luzon[17]) but the computational cost is considerable in terms of memory and/or computer-time and most simulations are characterized either by very constricting assumptions (e.g. on the geometry of the valley or on the wavelength of the propagating waves relative to the structure) or they are limited to low frequencies.

This paper presents an extension of the indirect boundary element method (IBEM) to the case of 3D scattering by 2D alluvial valleys, i.e. with waves arriving from outside the 2D plane which includes the cross-section of the valley, so the scattering is 3D. Such a method is potentially a useful tool to estimate site effects in valleys that for practical purposes can be considered 2D. This development was motivated by observations (King and Tucker,[18] Jongmans and Campillo[19]) of correlations between local amplification and earthquake locations relative to the valley.

3D scattering by 2D structures ('2·5D scattering') has been studied by Luco *et al.*,[20] Pei and Papageorgiou[21] and Pedersen *et al.*[22] for topographies and by Khair *et al.*,[23,24] Liu *et al.*[25] and Pei and Papageorgiou[26]

for alluvial valleys. The advantages of the IBEM method presented in this paper is the combination of high accuracy and low computational cost. A detailed discussion of IBEM can be found in Sánchez-Sesma and Campillo,[27] Sánchez-Sesma et al.[28] or Sánchez-Sesma and Luzon.[17]

This paper is separated into two parts. The first one presents the extension of IBEM to the simulation of site effects in alluvial valleys where the incident waves arrive outside the 2D plane. The second part presents the application of the method to systematically study how azimuth and incidence of the incident waves influence local amplifications in alluvial valleys. The model used is that of the Ubaye Valley in the French Alps where azimuth dependence has been observed by Jongmans and Campillo.[19] The second part also contains a comparison between observed and theoretical spectral ratios.

## METHOD

The indirect boundary element method (IBEM) is based on an integral representation of wave fields. IBEM applied to diffraction by alluvial valleys are presented in recent papers by Sánchez-Sesma et al.[28] and Sánchez-Sesma and Luzon[17] and we refer to these two papers for a full description of the basic theory. In this section we will describe the method very briefly and focus on points relevant to the problem of three-dimensional scattering by two-dimensional structures.

Neglecting body forces, the displacement field in a domain $V$ with boundary $S$ occupied by an elastic material can be stated as (see e.g. Sánchez-Sesma and Campillo[29]):

$$u_i(\mathbf{x}) = \int_S \psi_j(\zeta) G_{ij}(\mathbf{x}, \zeta) \, dS_\zeta \qquad (1)$$

where $u_i(\mathbf{x})$ is the $i$th component of displacement at $\mathbf{x}$; $G_{ij}(\mathbf{x}, \zeta)$ is the Green function, i.e. the displacement in direction $i$ at $\mathbf{x}$ due to a point force in direction $j$ applied at the point $\zeta$; $\psi_j(\zeta)$ is the force density in direction $j$ at $\zeta$. $\psi_j(\zeta) \, dS_\zeta$ is therefore a force distribution on $S$. The integration is performed over the space variable $\zeta$. Equation (1) is valid both in $V$ and on $S$ because $\mathbf{u}$ is continuous across $S$ if $\psi$ is continuous on $S$ (Kupradze[30]).

We consider an elastic half space, $E$, with an elastic inclusion, $R$, as shown in Fig. 1. The two elastic media are in contact at the interface $\delta$. The total displacement $\mathbf{u}^E$ in the half space can be considered to be the superposition of the displacement $(u^{(d)})$ of the 'diffracted or scattered field' and the displacement $(\mathbf{u}^{(o)})$ of the 'free-field', i.e. the field in the absence of the irregularity

$$u_i^E = u_i^{(d)} + u_i^{(o)} \qquad (2)$$

where $\mathbf{u}^{(d)}$ can be expressed by the integral representation of eqn (1) over the surface that delimits the half
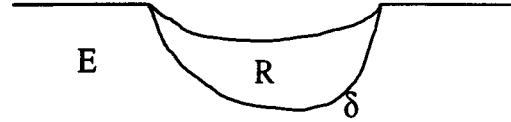


Fig. 1. Model of alluvial valley. The half-space $(E)$ and the valley $(R)$ are separated by the interface $\delta$.

space $E$. Equivalent expressions exist for tractions. In the inclusion $R$, the free-field is zero so total displacements and tractions are expressed by eqn (1) and its equivalent for tractions applied over the surface that delimits $R$. It is possible to find discrete expressions of displacements and tractions in $E$ and in $R$ when the free surface and $\delta$ are discretized into boundary elements with constant force density on each one.

Boundary conditions for the problem are

(1) zero-traction at the free surface
(2) continuity of displacement across $\delta$
(3) continuity of tractions across $\delta$

It is possible to express these boundary conditions by system of linear equations with the forces $\psi_j$ on each segment as the unknowns. The boundary conditions are evaluated at the source locations, so the number of unknowns equals the number of equations and the force densities are found by simple resolution of the system. Once the amplitude of the surface force is found for each element, the discrete version of eqn (1) can be applied to find the displacement of the refracted field at any location inside the valley. In the half space, the displacement of the free-field is added to that of the diffracted or scattered field to find the total displacement.

The calculation briefly described above is performed for each frequency and the synthetic seismograms are obtained by multiplication of a source function followed by a Fourier transform.

The 2·5D case is particular because although the scattering is three-dimensional, it is possible to represent the geometry of the structure in only two dimensions. The geometry of the problem is shown in Fig. 2. Plane waves are incident on a two-dimensional structure which is considered infinite in the direction of the $y$ axis. The incident waves arrive with an azimuth $\phi$ relative to the structure and an incidence $\theta$ to the vertical axis (see Fig. 2) and it propagates with a velocity $c$. The waves have an apparent velocity $c'$ along the $y$ axis

$$c' = \frac{c}{\sin\phi \sin\theta} \qquad (3)$$

For any two cross-sections perpendicular to the $y$ axis the wave field is identical but shifted in time, so the scattered wave field can be expressed by point sources that move parallel to the $y$ axis with a constant velocity $c'$ along the interfaces of the model. This approach has also been used by Luco et al.,[20] Khair et al.,[23,24] Pei and Papageorgiou[21,26] and Pedersen et al.[22] In the case of an
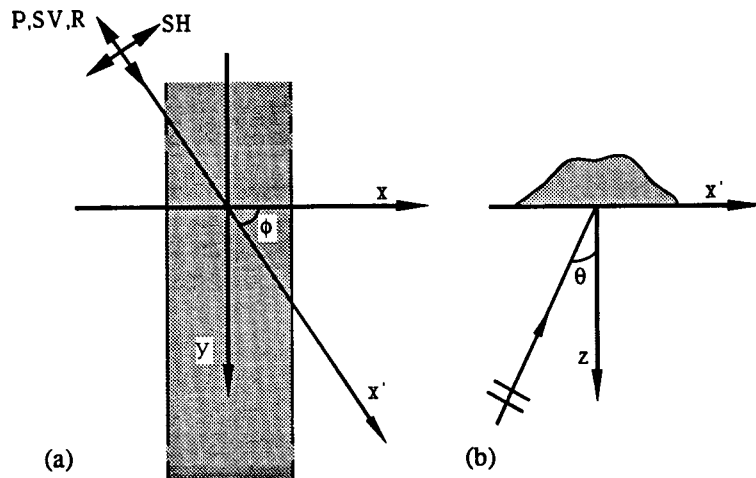
Fig. 2. Geometry of 2·5D scattering. (a) Horizontal plane, definition of azimuth $\phi$. (b) Vertical plane, definition of incidence $\theta$.

inclusion, the point sources move along the free surface and along the interface $\delta$.

We use compact, analytical expressions for Green functions for moving point sources in a full-space (Pedersen *et al.*[22]). Use of such full-space expressions is a way of significantly reducing computer time as compared to computations with half space Green functions. Possible unwanted boundary truncation effects can be avoided or minimized by discretizing the free surface out to a sufficient distance from the irregularity. The integration of the Green functions along each element is performed by Gaussian integration. For observation points located on a segment, the integrations are computed analytically.

## VERIFICATION OF THE METHOD

We verified the accuracy of the method by (1) transparency tests, (2) comparisons with known 2D solutions, and (3) comparison with other published results.

Transparency tests are comparisons of analytical solutions for displacements of plane waves propagating in a half space with the corresponding numerical simulations where the valley has a flat surface and a same material inside and outside the valley. Our results were within 1–2% of the analytical solutions.

The 2D case is a limiting case for the simulations (azimuth $\phi = 0$). A large number of 2D simulations

are now available for alluvial valleys. We compared our results with those of Sánchez-Sesma *et al.*[29] The two methods are strictly equivalent in the 2D case because the simulation method is similar and because the 2·5D Green functions for zero azimuth equal the 2D Green functions. The comparison showed that the differences in computed displacements of the two simulation methods are smaller than 1% of the amplitude of the incoming waves. Sánchez-Sesma *et al.*[29] show that their results correspond well to those of other authors and to analytical solutions so we will not discuss here the 2D case further.

Very few results are available for 3D scattering by 2D valleys. We have compared our results to those of Pei and Papageorgiou[26] because their results are presented in the time domain so the whole frequency range is considered in computations. The model is the one depicted in Fig. 3. The elastic parameters used are also given in Fig. 3. The plane waves incident upon the valley are of P, SH or SV type and they have an arbitrary azimuth and incidence angle to the valley. The source function used is a Ricker wavelet of 0·55 Hz central frequency. We verified our results on all Pei and Papageorgiou's[26] examples. The differences are very small (within 1–2%). An example of comparison between simulations is shown in Fig. 4, where the results are shown for incident SV waves with azimuth 60° and vertical incidence 30°. We also compared our results with those of Pei (personal communication) for a deeper
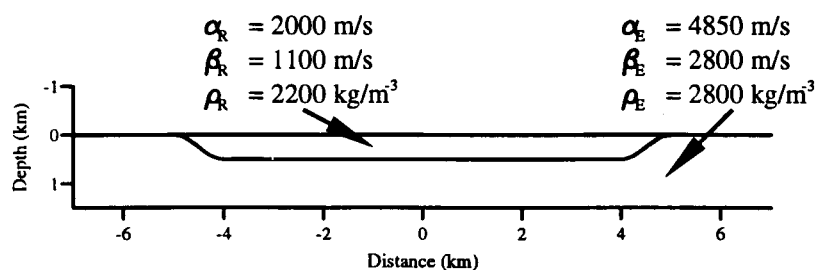


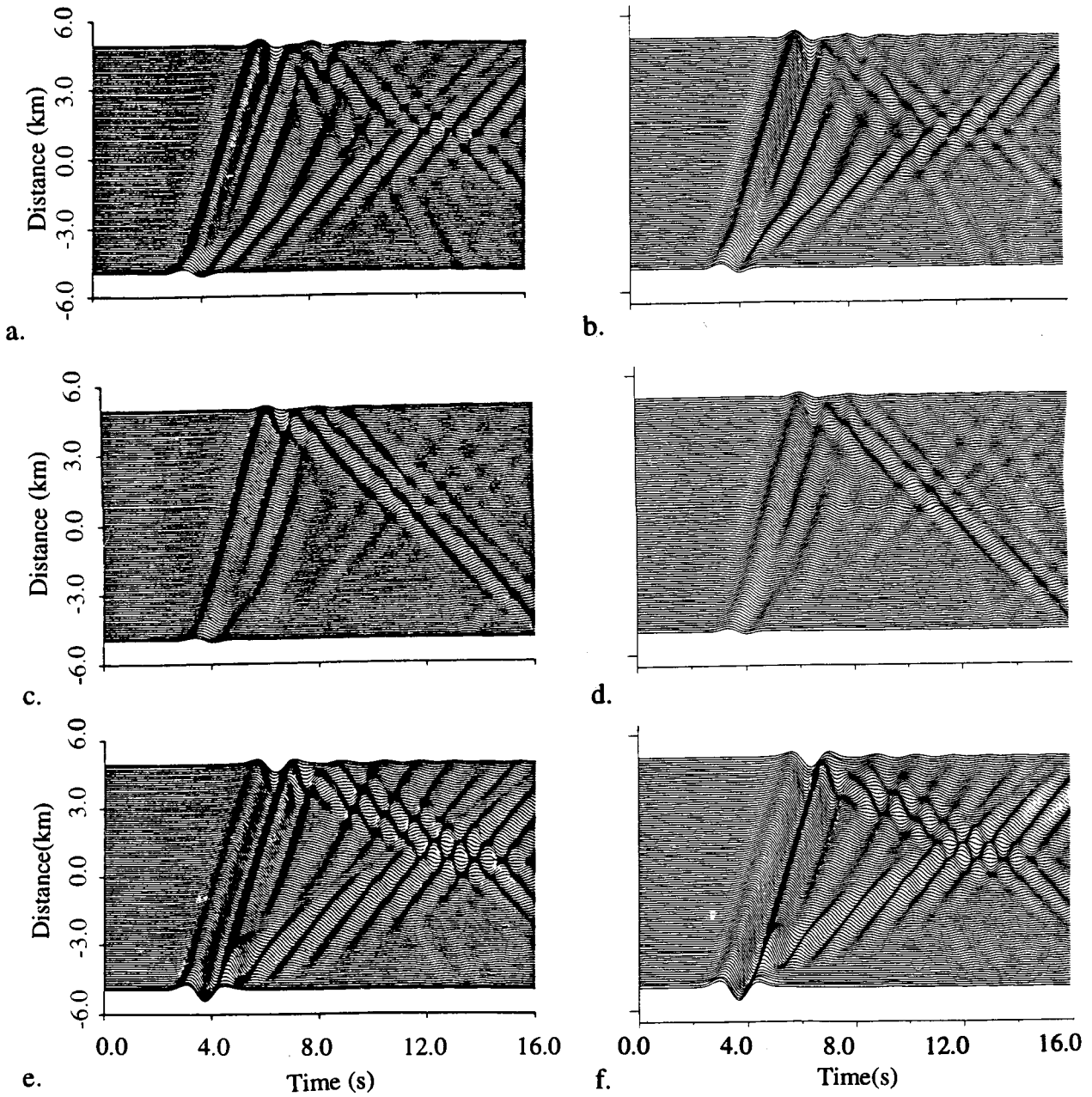Fig. 3. Model used for comparison of our results with those of Pei and Papageorgiou.[26]

**Fig. 4.** Comparison of our results (b, d, f) with those of Pei and Papageorgiou[26] (a, c, e). Incoming wave: SV wave with azimuth 30° and incidence 60°. (a), (b): $Ux$, displacement perpendicular to valley. (c), (d): $Uy$, displacement parallel to valley. (e) (f): $Uz$, vertical displacement.



$\alpha_R = 2000$ m/s
$\beta_R = 900$ m/s
$\rho_R = 1700$ kg/m$^{-3}$
$Q_R = 40$

$\alpha_E = 4600$ m/s
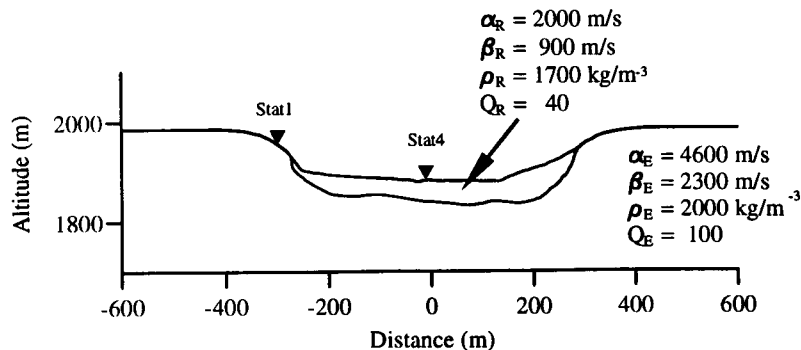$\beta_E = 2300$ m/s
$\rho_E = 2000$ kg/m$^{-3}$
$Q_E = 100$

**Fig. 5.** Simplified model of Ubaye Valley. Seismic stations are shown by triangles.

valley to assure that the good agreement between results was independent on the shape of the valley.

## RESULTS

### Simple model of Ubaye Valley

For the application of the method, we chose to study amplification across an alluvial valley for which local amplification is azimuth-dependent (Jongmans and Campillo[19]). The valley in question, the Ubaye Valley, is several kilometers long and narrow (approx. 600 m wide) alluvial deposit in the French Alps. The basin's geometry and seismic propagation velocities in the sediments and bedrock have been estimated by reflection and refraction seismic experiments and by inversion of Rayleigh wave dispersion (Jongmans et al.,[31] Jongmans and Campillo[19]).

The bedrock consists of unweathered limestone ($Vp =$ 4500–5500 m/s; $Vs = 2100$–2400 m/s). The deposits contain 3 units:

1. A surficial layer of recent alluvium from the Ubaye river and collovium from the shoulders of the valley, characterized by rapid lateral changes in propagation velocities ($Vp = 400$–700 m/s; $Vs = 150$–350 m/s) and locally internal layering.
2. An intermediate deposit ($Vp = 1600$–2300 m/s; $Vs = 500$–750 m/s).
3. A deep layer, probably consolidated moraines, which is present only in the central part of the valley ($Vp = 2850$–3200 m/s; $Vs = 900$–1300 m/s).

At the present stage, the method presented above can be used to simulate the seismic response of an alluvial valley without internal layering. We therefore constructed a simplified model of the valley that partly takes the internal layering of the loose sediments into account. At each point across the valley, the one-dimensional response was calculated using the wave propagation velocities and layer thicknesses immediately beneath the point. The thickness of an equivalent layer with average wave propagation velocities ($Vp = 2000$ m/s, $Vs = 900$ m/s) was calculated so the lowest resonance frequency of the one-layer model was equal to that of the three-layer model. The slope of the shoulders of the valley is taken into account in the final model, which is shown in Fig. 5.

An example of synthetic seismograms for the simplified model is shown in Fig. 6. The example (incident SV waves with azimuth 30° and incidence 40°) is chosen among many simulations made for the simplified Ubaye Valley model. The source function is a Ricker wavelet with a central frequency of 8 Hz and the stations are located across the valley from −355 to 350 m. The seismograms clearly show how the amplification pattern is dominated by surface waves propagating across the valley.
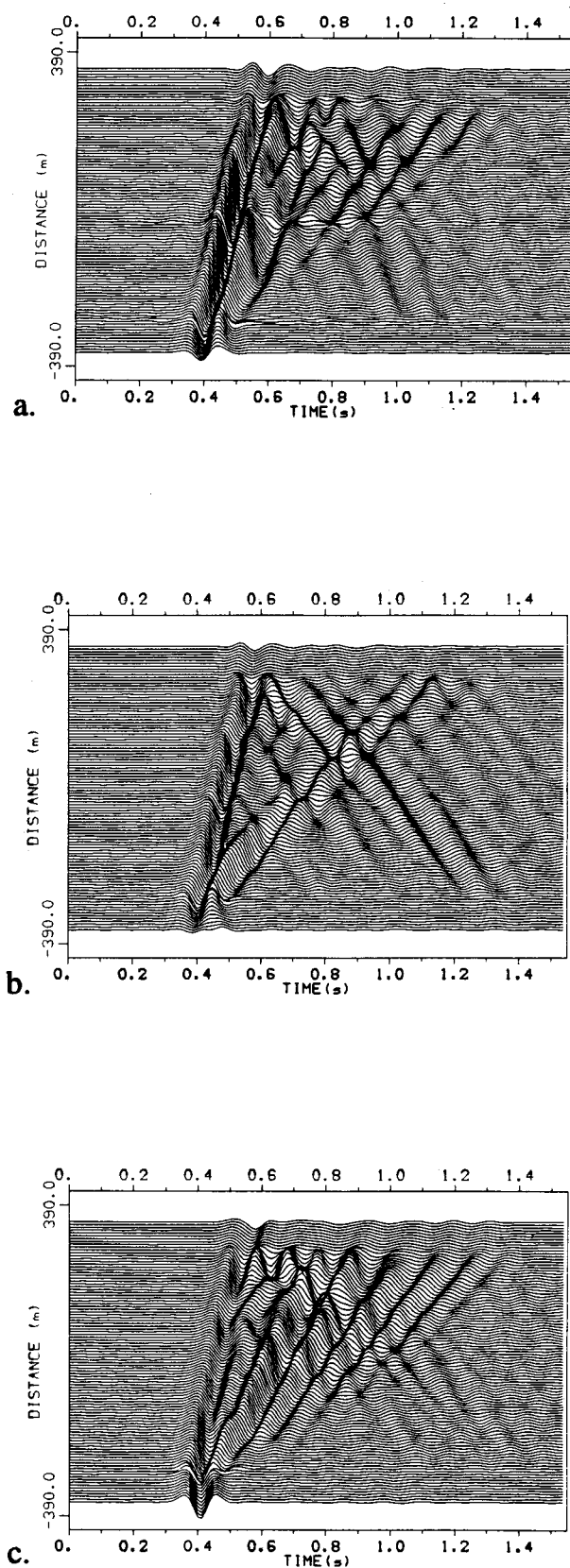


Fig. 6. Example of synthetic seismograms for Ubaye Valley due to incident waves of type SV, azimuth 30° and incidence 40°. (a) Ux, displacement perpendicular to valley. (b). Uy, displacement parallel to valley. (c) Uz, vertical displacement.

## Parametric study

We carried out a large number of simulations to quantitatively estimate how incidence ($\theta = 10°$, $20°$, $30°$, $40°$) and azimuth ($\phi = 0°$, $30°$, $60°$, $90°$, $120°$, $150°$, $180°$) influence the local amplification across the valley when the incoming waves are of type SV or SH and all other parameters (except azimuth, incidence and wave type) are constant. We studied horizontal, vertical and total amplification across the valley for one frequency and for frequency intervals. Other results are presented in terms of location in the valley and frequency of the maximum amplitudes. Selected results are shown for maximum amplitudes across the valley because this was the only parameter where we found systematic changes as a function of azimuth.

All amplitudes are normalized with the amplitude of the free-field $u^{(o)}$ (incident waves + reflection at the free surface). For SH waves these free-field amplitudes equal two for all incidence angles while they vary between 1·64 and 3·44 for SV waves ($\theta = 10°$: $u^{(o)} = 1·99$; $\theta = 20°$: $u^{(o)} = 1·97$; $\theta = 30°$: $u^{(o)} = 3·44$; $\theta = 40°$: $u^{(o)} = 1·64$). For all simulations, displacement amplitudes at each

station were computed for frequencies between 0 and 10 Hz. Figures 7–10 show these results: maximum amplitudes are displayed for each incidence angle as a function of azimuth and location across the valley. Figures 7 and 8 show these maximum values for horizontal and vertical motion, respectively, for incident SH waves. Corresponding results for incident SV waves are presented in Figs 9 and 10.

Even for fixed azimuth and incidence, the amplitude pattern across the valley is very complex. The figures nevertheless show some general trends:

1. Alternating large and small amplitudes across the valley for fixed azimuth and incidence angle.
2. Larger vertical displacement amplitudes and slightly smaller horizontal amplitudes for incoming SH waves that arrive with an azimuth of $60°-120°$ compared to the pure 2D case.
3. Smaller vertical displacement amplitudes and slightly higher horizontal amplitudes for incoming SV waves that arrive with an azimuth $60°-120°$ compared to the pure 2D case.
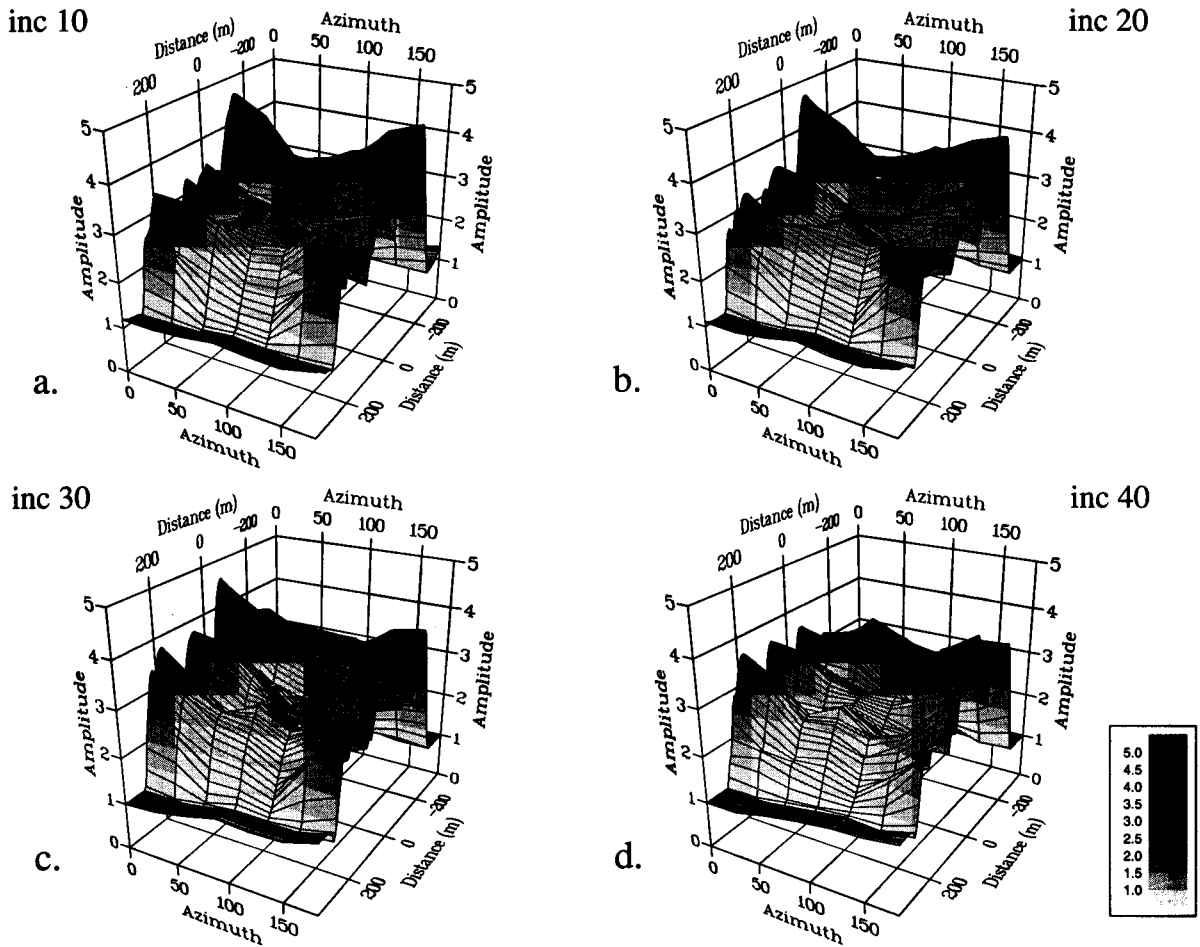4. Change of amplification pattern for incoming SV waves at critical incidence ($30°$).



Fig. 7. Maximum horizontal amplification of SH waves between 0 and 10 Hz as a function of distance across the valley and azimuth of the incoming waves. (a) Incoming waves with incidence $10°$. (b) Incoming waves with incidence $20°$. (c) Incoming waves with incidence $30°$. (d) Incoming waves with incidence $40°$.
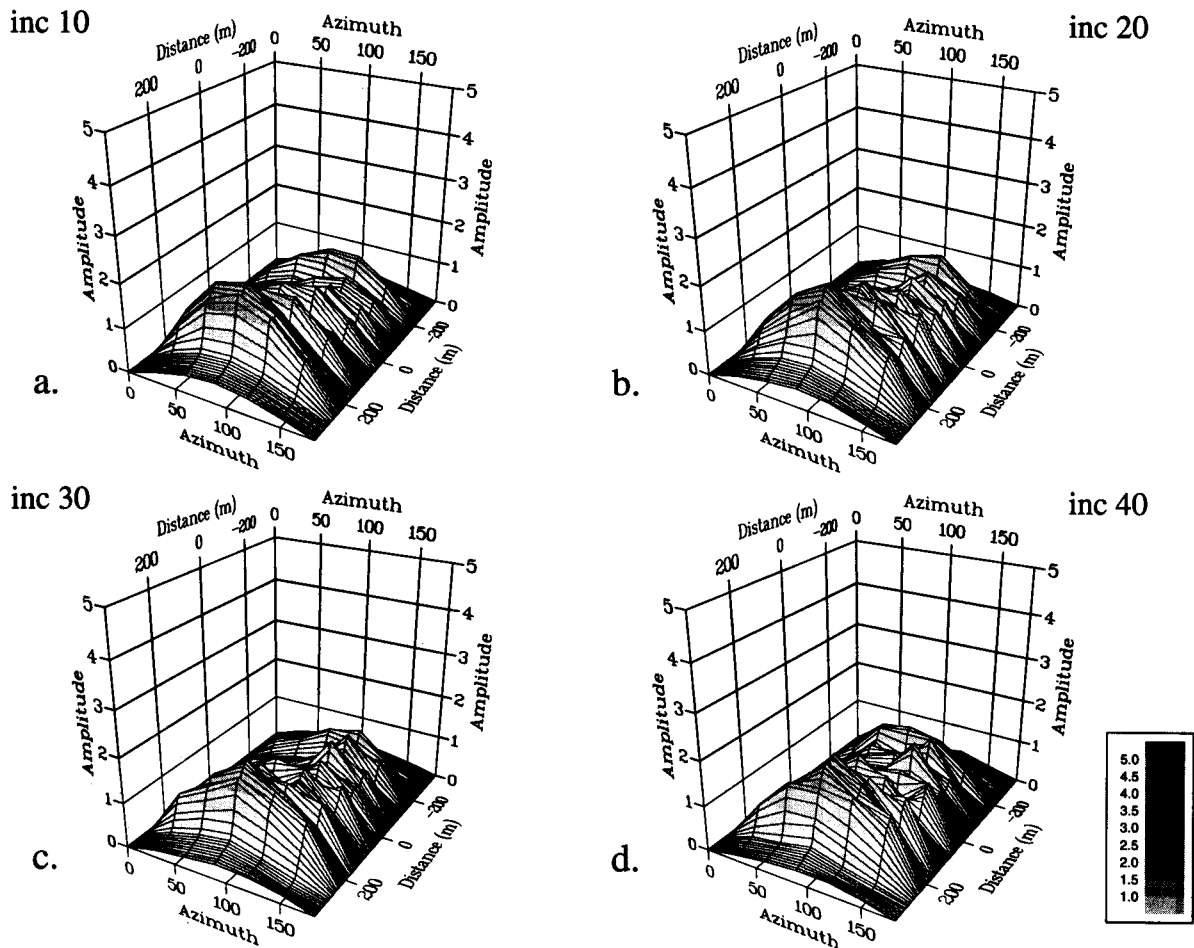
**Fig. 8.** Maximum vertical amplification of SH waves between 0 and 10 Hz as a function of distance across the valley and azimuth of the incoming waves. (a) Incoming waves with incidence 10°. (b) Incoming waves with incidence 20°. (c) Incoming waves with incidence 30°. (d) Incoming waves with incidence 40°.

The first point confirms results for the pure 2D case: the local amplification across the valley is dominated by interfering surface waves also when the incoming waves arrive outside the 2D plane. We confirmed this by $f-k$ analysis across the central stations in the valley and comparison of the amplification pattern in the $f-k$ domain with dispersion curves for Rayleigh and Love waves for a one-layer model of the central part of the valley. The $f-k$ image of the simulations is too coarse to identify individual modes but waves with propagation velocities similar to those of the fundamental Rayleigh and Love modes exist for all simulations. This is also an indication that at least some of the wave propagation in the valley takes place in the 2D plane, because plane waves propagating outside the 2D plane have a higher apparent velocity over the array of stations.

The dependence of maximum vertical displacement on wave type and azimuth also suggests that most of the surface waves in the valley propagate approximately in the 2D plane. If we consider the vertical displacement, Rayleigh waves propagating in the 2D plane will for incoming SH waves be more efficiently generated

at 90° azimuth (all incoming energy in the plane perpendicular to the valley) with coupling between horizontal and vertical displacement. The opposite is true for incoming SV waves where 90° azimuth implies an efficient generation of Love waves which have no displacement on the vertical component. This interpretation is nevertheless far too simplistic to explain the complete amplification pattern in the valley and is of limited use for practical purposes.

Other indications of mostly 2D propagation in the valley are of physical character. In fact, the incoming waves can be expected to be refracted *into* the valley because of the impedance contrast. The Green functions calculated for points in the valley show that they approach the 2D solutions with almost complete decoupling of P–SV and SH motions when $c'$ (i.e. the speed of the moving point sources) is significantly bigger than the propagation velocities in the valley. This effect also depends on the impedance contrast between the valley and the half space.

Even though some phenomena of the local amplification may indicate that generated waves in the valley mainly propagate in a direction perpendicular to the
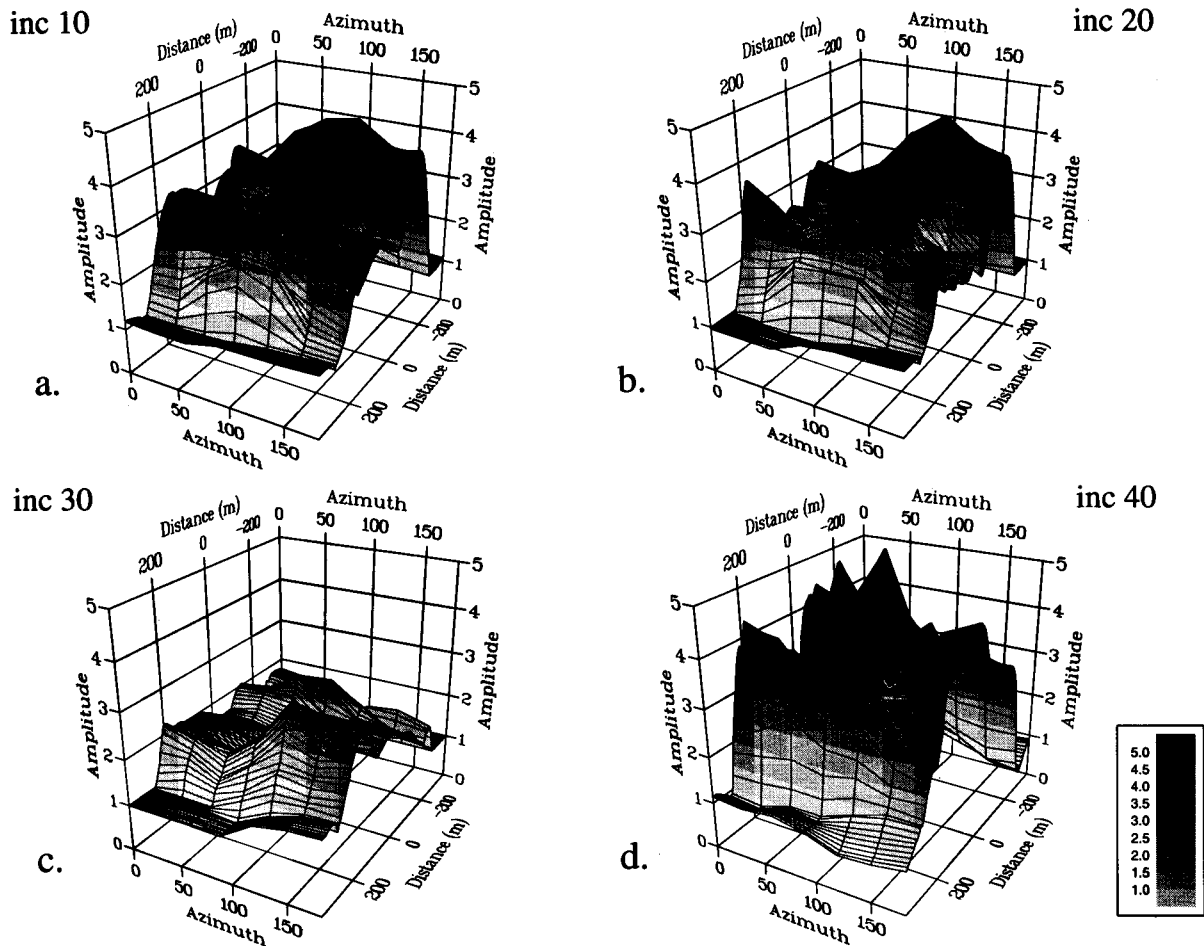
**Fig. 9.** Maximum horizontal amplification of SV waves between 0 and 10 Hz as a function of distance across the valley and azimuth of the incoming waves. (a) Incoming waves with incidence 10°. (b) Incoming waves with incidence 20°. (c) Incoming waves with incidence 30°. (d) Incoming waves with incidence 40°.

valley, the final amplification pattern is also controlled by the boundary conditions introduced by the free-field. Figures 7–10 show that it does not seem possible for example to predict the amplification pattern for different azimuths, knowing the 2D solution of the response. Furthermore, if only one frequency is considered, the influence of azimuth is less clear than when a whole frequency range is available. This is illustrated by Fig. 11 which is the equivalent of Fig. 7 (horizontal amplification for incoming SH waves) for a single frequency, 10 Hz.

Finally, the change of amplification pattern at the critical angle of incidence for SV waves is the expression of significant changes in boundary conditions. Incident SV waves on a free surface (e.g. Aki and Richards[32]) with incidence angles *below* critical produce reflected P and SV waves. *At* critical incidence a diffracted P wave propagates horizontally and has a large amplitude. *Beyond* critical incidence, such P waves are inhomogeneous and also propagate horizontally. Observations of damage patterns at a hill-profile that correlated well with the critical angle of SV waves were reported by Kawase and Aki.[33] Numerical simulations (e.g. Bouchon,[34]

Mateos *et al.*[35]) show significant amplifications related to incoming SV waves at certain incidences in layered media as well. These studies pointed out significant amplitudes for a SP phase, formed by diffracted P waves and the incoming and reflected SV waves. However, such a *wave system* is a by-product of incident SV waves, therefore it can only exist with its carrier, i.e. the incident SV wave. For this reason, the resonance in a shallow alluvial basin will be controlled by local surface waves.

### Comparison between observed and theoretical spectral ratios

Jongmans and Campillo[19] studied the wave amplification in Ubaye Valley by the use of a five station array. They calculated spectral ratios between stations in the valley (stations 2–5) and a hard-rock reference station (station 1).

The influence of surficial layers is ignored in the simulations so the simplified model of Ubaye Valley is not sufficiently detailed to model observations. It is
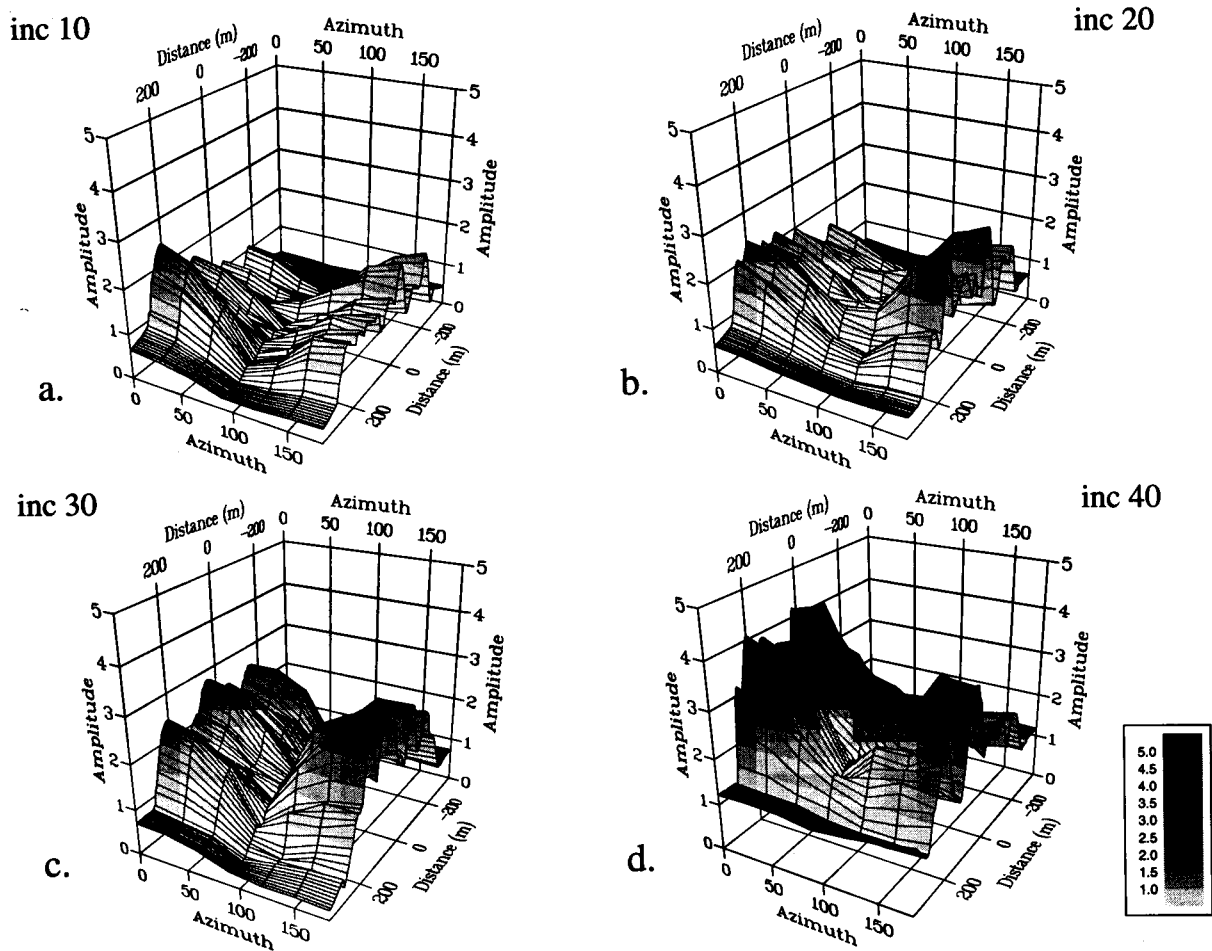
inc 10

inc 20

inc 30

inc 40



Fig. 10. Maximum vertical amplification of SV waves between 0 and 10 Hz as a function of distance across the alley and azimuth of the incoming waves. (a) Incoming waves with incidence 10°. (b) Incoming waves with incidence 20°. (c) Incoming waves with incidence 30°. (d) Incoming waves with incidence 40°.

nevertheless interesting to compare observed spectral ratios with theoretical ones for the station in the valley (station 4) which is expected to be the least influenced by the surficial layers. They are under this particular station shallow and approximately horizontal. The locations of station 1 and 4 are shown in Fig. 5.

Earthquakes recorded by the array (Jongmans and Campillo[19]) were shallow and their hypocenters relative to the site fell into 3 groups:

1. Approximately 5 km north–north-west.
2. Approximately 20 km east.
3. Approximately 30 km east–south-east.

Jongmans and Campillo[19] show that the measured spectral ratios are different among these three groups.

In terms of azimuth relative to the structure, group 1 is at 0°, group 2 is at 120° and group 3 is at 150°. The incidence angles of the waves relative to the structure is expected to be smaller for group 1 than for groups 2 and 3 because group 1 is approximately located *under* the valley. In the earthquake records, the incoming waves are not polarized in a single plane. For each group we therefore used results of simulations with two wave

types (SH and SV) and three incidence angles. The theoretical spectral ratio station 4/station 1 was found as the square-root of S4/S1 where S denotes the added energy spectra of the six simulations used for the group. The parameters of the simulations were the following:

1. Group 1: SH and SV waves with azimuth 0° and incidence angles 0°, 20° and 40°.
2. Group 2: SH and SV waves with azimuth 120° and incidence angles 20°, 40° and 60°.
3. Group 3: SH and SV waves with azimuth 150° and incidence angles 20°, 40° and 60°.

The topography adjacent to the valley was taken into account out to a distance of approx. 1 km from the edge of the valley. This does not significantly change wave propagation in the valley but it significantly affects spectral amplitudes at the location that corresponds to station 1.

Figure 12 shows the comparison between observed and theoretical spectral ratios. The observed tendency of increasing spectral ratio with azimuth is accounted for by the simulations which show that this tendency
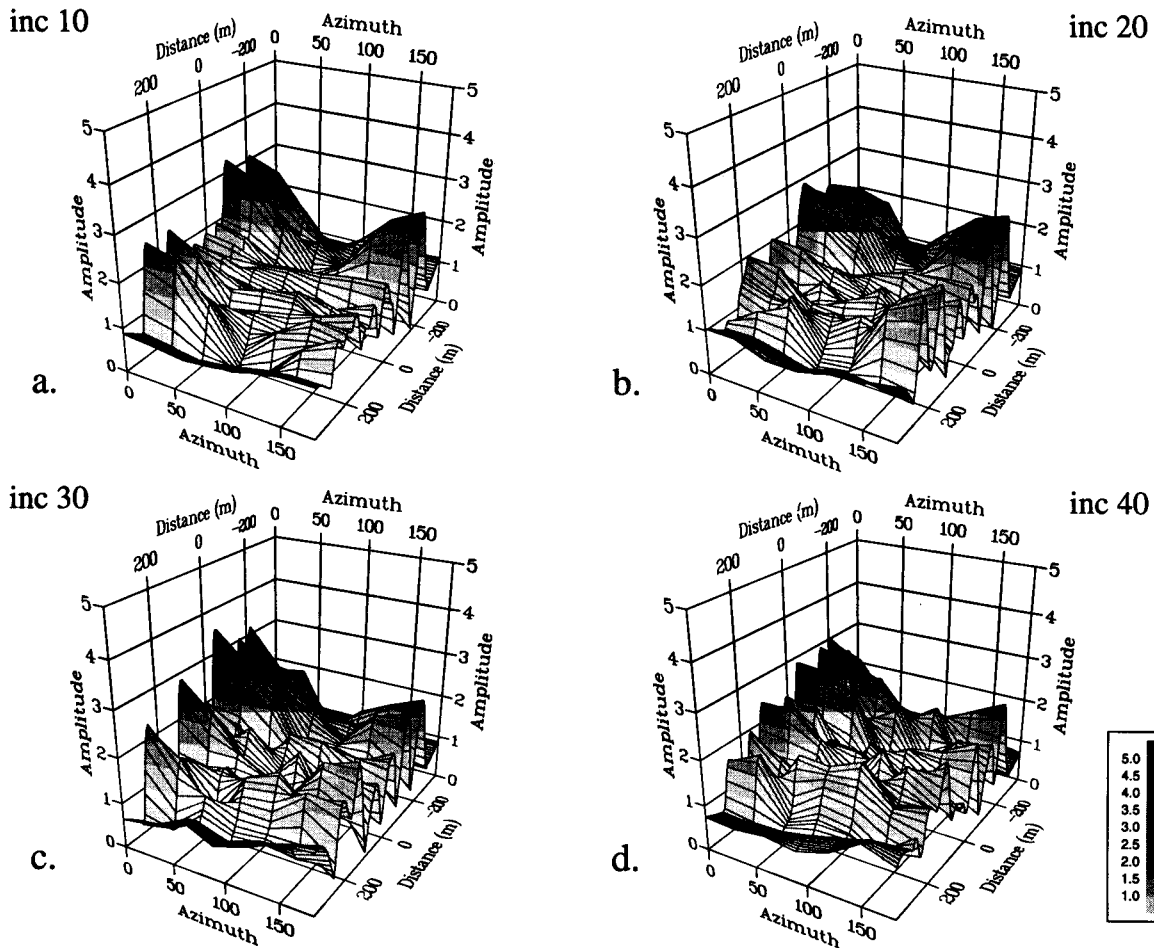
**Fig. 11.** Horizontal amplification of SH waves at 10 Hz as a function of distance across the valley and azimuth of the incoming waves. (a) Incoming waves with incidence 10°. (b) Incoming waves with incidence 20°, (c) Incoming waves with incidence 30°. (d) Incoming waves with incidence 40°.

is due to a shadow effect at station one for large azimuths and incidence angles. The general shape of the theoretical curves is in good agreement with the observed ones, considering that we use a simplified model and plane-polarized incident waves.

## CONCLUSIONS

Our results show significant effects of the azimuth of incoming seismic waves, but in such a way that it is not easily predictable. Both in the pure 2D case and when the incident waves arrive outside the 2D plane, the amplification is due to the interference of different waves, in particular surface waves, so even small changes in boundary conditions will change the interference and therefore the local amplification across the valley. General trends can be identified for some parameters (maximum total, horizontal and vertical amplitude in a frequency interval), but other parameters such as the frequency or station location of the maximum amplifications have no systematic variation with azimuth or incidence angle. On the other hand,

our simulations and comparisons with observed spectral ratios in Ubaye Valley show that 2·5D modeling is necessary for a complete and realistic description of the local amplification across alluvial valleys.

The simulations furthermore show that azimuth effects are present both inside and outside the valley, so spectral ratios measured relative to a reference station can be biased. In the example of Ubaye valley, the reference station would for certain azimuths of the incident waves be located in a 'shadow zone' so absolute amplifications in the valley would be overestimated.

The application of the IBEM extension to 2·5D scattering shows that it is a powerful method because it combines accuracy with low computational costs. In the examples presented, the simulations between 0 and 10 Hz consumed less than 2 h CPU on a medium-sized workstation (6–9 Mflops). The CPU-time was approx. 22 h for each total simulation (0–37 Hz), with the high frequency part of the calculation (20–37 Hz, 11 CPU) carried out on a larger workstation (25–30 Mflops). The method does therefore seem very promising both as a practical tool for interpretation
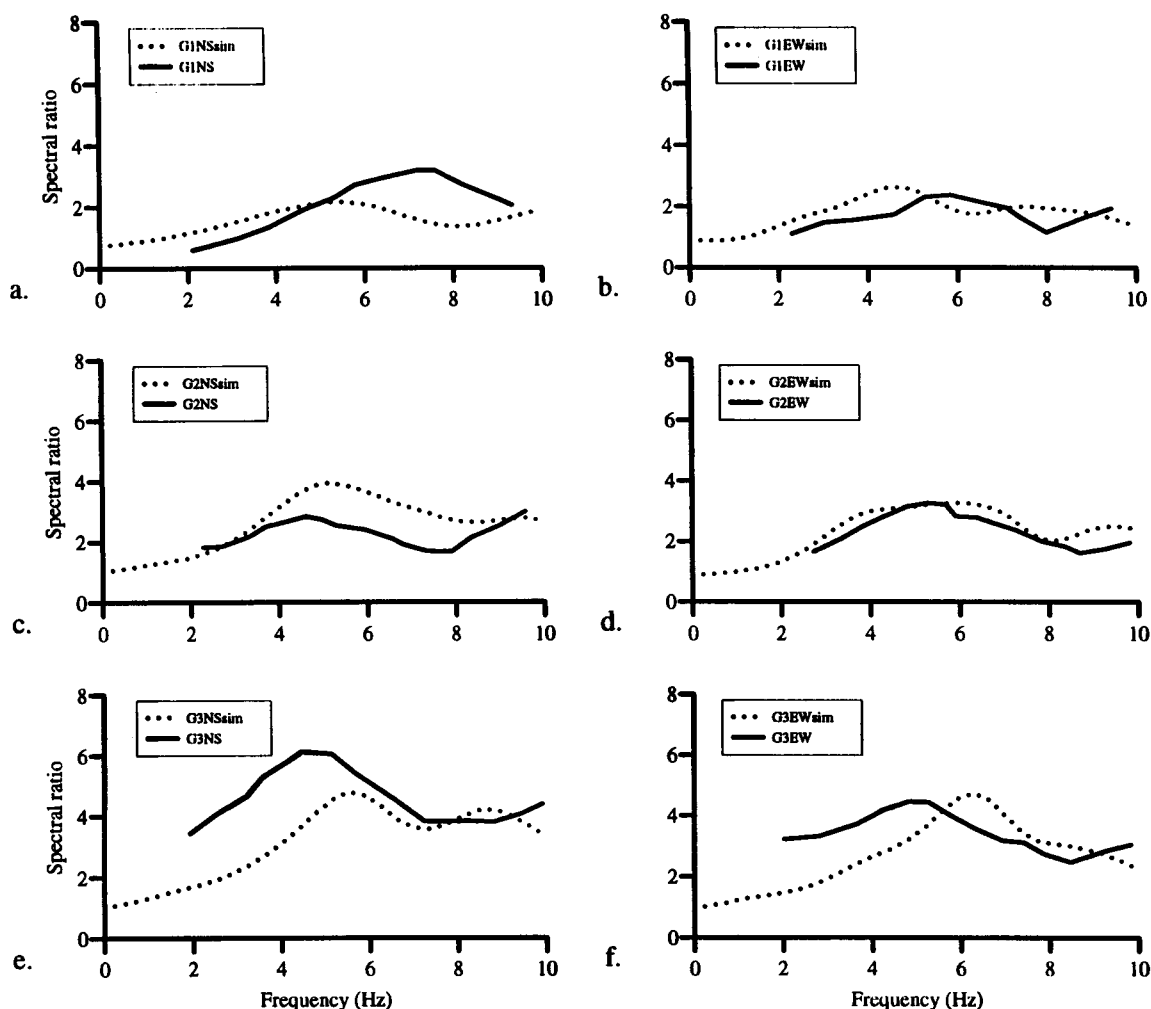
Fig. 12. Comparison between observed (solid lines) and theoretical (dotted lines) spectral ratios station 4/station 1. (a) Group 1, NS component. (b) Group 1, EW component. (c) Group 2, NS component. (d) Group 2, EW component. (e) Group 3, NS component. (f) Group 3, EW component.

of data and for extension to for example more complex geometries.

## REFERENCES

1. Rogers, A. M., Borcherdt, R. D., Covington, P. A. & Perkins, D. M. A comparative ground response study near Los Angeles using recordings of Nevada nuclear tests and the 1971 San Fernando earthquake. *Bull. Seism. Soc. Am.*, **74**, 1984, 1925–1949.
2. Tucker, B. E. & King, J. L. Dependence of sediment-filled valley response on input amplitude and valley properties. *Bull. Seism. Soc. Am.*, **74**, 1984, 153–165.
3. Singh, S. K., Mena, E. & Castro, R. Some aspects of source characteristics of the 19 September 1985 Michoacan earthquake and ground motion amplification in and near Mexico City from strong motion data. *Bull. Seism. Soc. Am.*, **78**, 1988, 451–477.
4. Jongmans, D. & Campillo, M. The 1983 Liège earthquake: damage distribution and site effects. *Earthquake spectra*, **6**, 1990, 713–737.
5. Borcherdt, R. D. & Glassmoyer, G. On the characteristics of local geology and their influence on ground motions generated by the Loma Prieta earthquake in the San Francisco Bay region, California. *Bull. Seism. Soc. Am.*, **82**, 1992, 603–641.
6. Gutierrez, C. & Singh, S. K. A site effect study in Acapulco, Guerrero, Mexico: comparison of results from strong-motion and microtremor data. *Bull. Seism. Soc. Am.*, **82**, 1992, 642–659.
7. Bard, P.-Y. & Bouchon, M. The seismic response of sediment-filled valleys. Part 1. The case of incident SH waves. *Bull. Seism. Soc. Am.*, **70**, 1980, 1263–1286.

8. Bard, P.-Y. & Bouchon, M. The seismic response of sediment-filled valleys. Part 2. The case of incident P and SV waves. *Bull. Seism. Soc. Am.*, **70**, 1980, 1921–1941.

9. Kawase, H. & Aki, K. A. A study on the response of a soft basin for incident S, P and Rayleigh waves with special reference to the long duration observed in Mexico City. *Bull. Seism. Soc. Am.*, **79**, 1989, 1361–1382.

10. Phillips, W. S., Kinoshita, S. & Fujiwara, H. Basin-induced Love waves observed using the strong-motion array at Fuchu, Japan. *Bull. Seism. Soc. Am.*, **83**, 1993, 64–84.

11. Sánchez-Sesma, F. J., Pérez-Rocha, L. E. & Reinoso, E. Ground motion in Mexico City during the April 25, 1989, Guerrero earthquake. *Tectonophysics*, **218**, 1993, 127–140.

12. Lee, J.-J. & Langston, C. A. Wave propagation in a three-dimensional circular basin. *Bull. Seism. Soc. Am.*, **73**, 1983, 1637–1653.

13. Sánchez-Sesma, F. J. Diffraction of elastic waves by three-dimensional surface irregularities. *Bull. Seism. Soc. Am.*, **73**, 1983, 1621–1636.

14. Sánchez-Sesma, F. J., Pérez-Rocha, L. E. & Chávez-Pérez, S. Diffraction of elastic waves by three-dimensional surface irregularities. Part II. *Bull. Seism. Soc. Am.*, **79**, 1989, 101–112.

15. Frankel, A. & Vidale, J. A three-dimensional simulation of seismic waves in the Santa Clara Valley, California, from a Loma Prieta aftershock. *Bull. Seism. Soc. Am.*, **82**, 1992, 2045–2074.

16. Rial, J. A. Seismic wave resonances in 3D sedimentary basins, *Geophys. J. Int.*, **99**, 1989, 81–90.

17. Sánchez-Sesma, F. J. & Luzón, F. Seismic response of three-dimensional alluvial valleys for incident P, S and Rayleigh waves. *Bull. Seism. Soc. Am.*, **85**, 1995, 269–284.

18. King, J. L. & Tucker, B. E. Observed variations of earthquake motion across a sediment-filled valley. *Bull. Seism. Soc. Am.*, **74**, 1984, 137–151.

19. Jongmans, D. & Campillo, M. The response of the Ubaye Valley (France) for incident SH and SV waves: comparison between measurements and modeling. *Bull. Seism. Soc. Am.*, **83**, 1993, 907–924.

20. Luco, J. E., Wong, H. L. & De Barros, F. C. P. Three-dimensional response of a cylindrical canyon in a layered half-space. *Int. J. Earthq. Eng. Struct. Dyn.*, **19**, 1990, 799–817.

21. Pei, D. & Papageorgiou, A. S. Three-dimensional response of an infinitely long cylindrical canyon to obliquely incident seismic waves, abstract. *Seism. Res. Lett.*, **64**, 1993, 27.

22. Pedersen, H. A., Sánchez-Sesma, F. J. & Campillo, M. Three-dimensional scattering by two-dimensional topographies. *Bull. Seism. Soc. Am.*, **84**, 1994, 1169–1183.

23. Khair, K. R., Datta, S. K. & Shah, A. H. Amplification of obliquely incident seismic waves by cylindrical alluvial valleys of arbitrary cross-sectional shape. Part I. Incident P and SV waves. *Bull. Seism. Soc. Am.*, **79**, 1989, 610–630.

24. Khair, K. R., Datta, S. K. & Shah, A. H. Amplification of obliquely incident seismic waves by cylindrical alluvial valleys of arbitrary cross-sectional shape. Part II. Incident SH and Rayleigh waves. *Bull. Seism. Soc. Am.*, **81**, 1991, 346–357.

25. Liu, S. W., Datta, S. K. & Bouden, M. Scattering of obliquely incident seismic waves by a cylindrical valley in a layered half-space, *Int. J. Earthq. Eng. Struct. Dyn.*, **20**, 1991, 859–870.

26. Pei, D. & Papageorgiou, A. S. Study of the response of cylindrical alluvial valleys of arbitrary cross-section to obliquely incident seismic waves using the discrete wave-number boundary element method. In *Soil Dynamics and Earthquake Engineering VI*, eds. A. S. Cakmak and C. A. Brebbia, Comp. Mech. Publications — Elsevier Appl. Sc., Southampton-London, 1993, pp. 149–161.

27. Sánchez-Sesma, F. J. & Campillo, M. Topographic effects for incident P, SV, and Rayleigh waves. *Tectonophysics*, **218**, 1993, 113–125.

28. Sánchez-Sesma, F. J., Ramos-Martinez, J. & Campillo, M. An indirect boundary element method applied to simulate the seismic response of alluvial valleys for incident P, S and Rayleigh waves. *Earthq. Eng. Struct. Dyn.*, **22**, 1993, 279–295.

29. Sánchez-Sesma, F. J. & Campillo, M. Diffraction of P, SV and Rayleigh waves by topographical features: a boundary integral formulation. *Bull. Seism. Soc. Am.*, **81**, 1991, 2234–2253.

30. Kupradze, V. D. Dynamical problems in elasticity. In *Progress in Solid Mechanics*, Vol. 3, eds. I. N. Sneddon and R. Hill. North-Holland, Amsterdam, 1963.

31. Jongmans, D., Campillo, M. & Demanet, D. The use of surface wave inversion and seismic reflection methods for engineering applications. In *Proc. 6th Int. Cong. I.A.E.G.*, Amsterdam, 6–10 August, 1990, Vol. 2, pp. 979–985.

32. Aki, K. & Richards, P. G. *Quantitative Seismology*. W. H. Freeman, San Francisco, 1980, pp. 123–163.

33. Kawase, H. & Aki, K. Topography effect at the critical SV-wave incidence: Possible explanation of damage pattern by the Whittier narrows, California, earthquake of 1 October 1987. *Bull. Seism. Soc. Am.*, **80**, 1990, 1–22.

34. Bouchon, M. The importance of the surface or interface P wave in near-earthquake studies. *Bull. Seism. Soc. Am.*, **68**, 1978, 1293–1311.

35. Mateos, J. L., Flores, J., Novaro, O., Alvarez-Tostado, J. M. & Seligman, T. H. Generation of inhomogeneous P waves in a layered medium. *Tectonophysics*, **218**, 1993, 247–256.